ELSEVIER

Journal of Fluids and Structures 24 (2008) 1216–1226

JOURNAL OF FLUIDS AND STRUCTURES

www.elsevier.com/locate/jfs

# Flow control in flow–structure interaction

R. Galvao[a], E. Lee[a], D. Farrell[a], F. Hover[a], M. Triantafyllou[a,*], N. Kitney[b], P. Beynet[b]

[a]*Massachusetts Institute of Technology, 77 Massachusetts Avenue, Cambridge, MA 02139, USA*
[b]*BP Exploration, Middlesex TW16 7LN, UK*

Received 23 January 2008; accepted 11 July 2008
Available online 31 October 2008

**Abstract**

We employ passive flow control using two-dimensional hydrofoils to reduce vortex-induced vibrations (VIV) and drag on a cylinder of circular cross-section. We test the hypothesis that by using foils to bend the streamlines around the cylinder, and hence forcing the flow to approach potential flow-like patterns VIV and drag will be reduced. A systematic parametric search, first using groups of two and then four foils, shows that it is possible to completely eliminate vibrations and reduce the drag coefficient to about $C_d = 0.50$ at sub-critical Reynolds numbers. This parametric search is conducted in conjunction with force measurement and particle image velocimetry on a fixed towed cylinder. The effectiveness of the foils in regards to VIV was further tested with an apparatus allowing free transverse vibrations of a towed cylinder.


*Keywords:* Vortex-induced vibrations; Flow control

## 1. Introduction

Vortex-induced vibrations (VIV) of elastically mounted bluff bodies and long flexible structures with bluff cross-sections can constitute a major problem for applications, especially in the ocean (Zdravkovich, 1997; Triantafyllou et al., 2003). The mechanisms of vortex formations and the resulting flow–structure interaction are of great interest to theoreticians and experimentalists. The problem of VIV of a circular cylinder has become the canonical problem of flow instability and flow–structure interaction (Sarpkaya, 1979, 2004; Bearman, 1984; Williamson and Govardhan, 2004). Both passive and active means of suppressing the formation of vortices have been studied extensively (Grimminger, 1945; Zdravkovich, 1980; Every et al., 1982; Jacobsen, 1996; Zdravkovich, 1997; Hoerner and Sighard, 1992). There are two basic mechanisms of inhibiting vortex formation to be considered. The first is a two-dimensional mechanism in which the average velocity profile behind the cylinder is altered to prevent the spontaneous emergence of vortical patterns due to the flow instability of the velocity profile; a small diameter rod placed parallel to and in the wake of the main cylinder, for example, can prevent vortex formation near the cylinder (Strykowski and Sreenivasan, 1990). The second is a three-dimensional mechanism through which a de-correlation of the separating flow is imposed; strakes,

*Corresponding author. Tel.: +1 617 253 4335.
*E-mail address:* mistetri@mit.edu (M. Triantafyllou).

0889-9746/$ - see front matter © 2008 Elsevier Ltd. All rights reserved.
doi:10.1016/j.jfluidstructs.2008.07.006

for example, have been found to be successful at preventing vortex formation, but at the expense of an increase in the average drag force (Zdravkovich, 1980).

Flow control in separated flows around bluff bodies holds the promise to eliminate unsteady transverse loads while reducing drag. If one views the potential flow as an ideal target at high Reynolds number, flow control can be used to force flow patterns to resemble those of the corresponding potential flow; the question is whether this is at all possible and to what extent. For a circular cylinder, such modification would indeed result in steady loads, and hence no VIV and very small (only frictional) drag forces.

In this study, the possibility of altering the flow around a circular cylinder by attaching combinations of flow directing hydrofoils is considered. These foils allow for alteration of the flow to produce streamlines more closely resembling potential flow patterns. Grimminger (1945) has used vanes to achieve the same effect. In this study, a number of approaches were studied through the use of two and then four symmetric hydrofoils, with some configurations assisted by a triangular fairing attachment. Results from this work demonstrate that values for drag coefficients can be brought down to 0.5–0.7 over the range of speeds tested. This leads to the conclusion that drag reduction in combination with VIV suppression is possible using hydrofoils.

## 2. Experimental procedure

### 2.1. Small scale force and PIV experiments

Experiments were conducted in a 2.4 m × 0.75 m × 0.75 m glass-wall water tank equipped with a carriage able to move along the length of the tank (Farrell, 2007). The main structural component of the carriage system is a rolling platform mounted above the tank (Fig. 1). An aluminum cylinder with a 3.81 cm diameter and hydrofoils made of epoxy-coated foam were used to form the test object. The mounting mechanism for the test object was attached to the load side of a six-axis load cell from JR3, Inc., with a linear load capacity of 110 N and moment capacity of 5.65 N m. The base of this force sensor was attached to the end of a cantilever beam which could driven in the horizontal plane by a pair of linear servo motors with 0.18 m range of travel. The amplified force sensor output was differentially captured at 1 kHz with a National Instruments USB-6211 DAQ card.

A particle image velocimetry (PIV) system was integrated into the assembly by mounting a high-speed LaVision Imager Pro camera to the platform directly behind the test object. The PIV system utilized makes use of a Quantronix Nd:YLF laser. A lens was used to disperse the laser light into a sheet that was projected perpendicular to the test structure. High-speed images within the range of 450–480 frames per second of illuminated particles added to the tank's water with a mean size of 43 μm. The DaVis La Vision PIV package was used to process these images and determine the flow vector field. A 32 × 32 window size with an average of eight particles within a processing window was used. These parameters provide an estimated error in reported velocities of approximately 4% (Willert and Gharib, 1991).

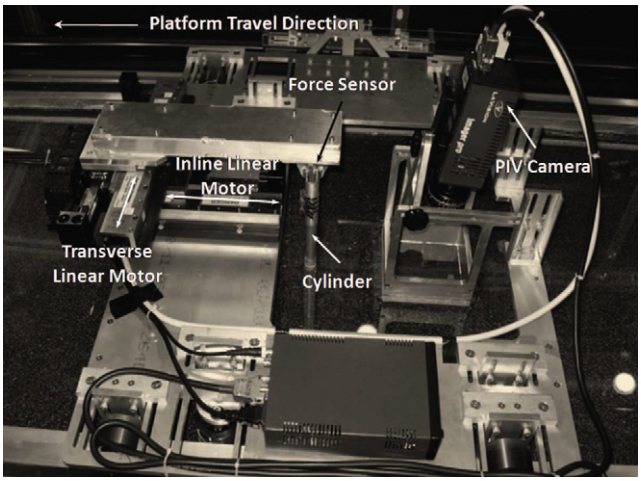


Fig. 1. The platform traveling along the length of the tank incorporates the various components shown.

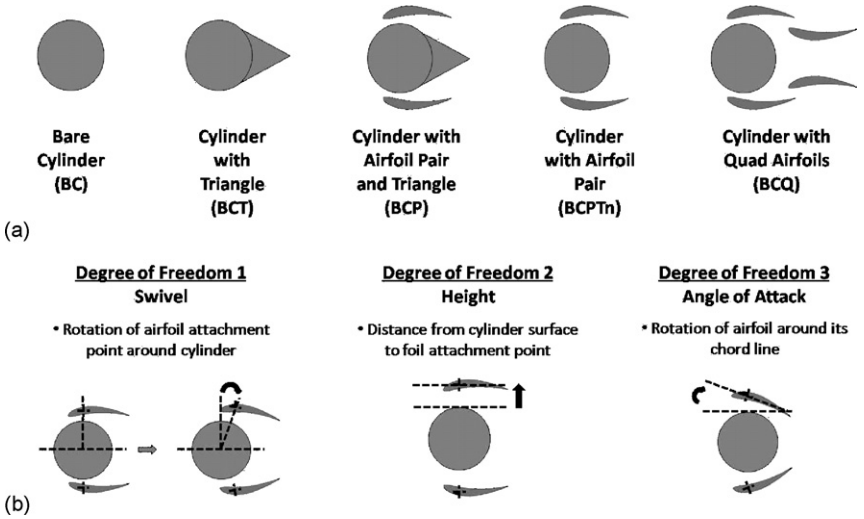


Fig. 2. A diagram is shown of (a) the modifications made to a bare cylinder and (b) the controllable parameters of these configurations.

A bare aluminum cylinder of 3.81 cm diameter was used as a control case. Modifications were made to this cylinder, such as the addition of a triangular fairing and hydrofoils. The triangular fairing was attached directly onto the downstream side of the cylinder and the hydrofoils were attached to the cylinder by means of specially made C-clamps that clamped onto the cylinder. These clamps had insert holes drilled through them in a circumferential pattern at various radial distances from the center of the cylinder. Hydrofoils with a E423 profile with chord lengths of 3.18 and 2.41 cm were made from epoxy hardened foam. A threaded post was embedded in both ends of each foil and served as a means of attaching the foils between the two C-clamps situated at opposing ends of the cylinder by using the insert holes and a securing nut.

A number of different foil configurations were tested and are depicted in Fig. 2. The cylinder, with and without the triangular fairing, was further modified by attaching a pair of hydrofoils. Each foil was attached in a manner to have it situated over the poles of the cylinder meaning the locations at which highest flow speed is attained. Furthermore, another test performed had two pairs of hydrofoils with different chord lengths simultaneously attached without the fairing. The pair with the smaller chord length was attached downstream of the flow directly behind the cylinder while the larger pair was attached as previously mentioned. The test object was towed along the length of the tank while force data in the inline and transverse directions were collected in addition to flow visualization of the wake directly behind the object. All tests were conducted at a Reynolds number of $8.5 \times 10^3$ based on the cylinder diameter.

Three major parameters were defined for the cylinder and hydrofoil system. First, the attachment location of the hydrofoil can be located anywhere along the circumference of the cylinder. This parameter is called the swivel angle; a value of zero degrees places the attachment points directly above the poles of the cylinder with angle increasing as the attachment point is rotated closer to the downstream stagnation point. Second, the height of the hydrofoils is defined as the distance of the hydrofoil attachment point from the cylinder surface. The third parameter is the angle of attack of the hydrofoils defined relative to the free-stream. The various configurations that will be discussed in this paper are defined as follows:

- BC: Bare cylinder with a diameter ($D$) of 3.81 cm.
- BCT: BC modified with a triangular fairing of extension length $D$.
- BCP: BCT with pair of hydrofoils (chord of 3.18 cm) positioned at a height of $1/3 \times D$, swivel angle of $10^\circ$ and angle of attack of $0^\circ$.
- $\text{BCPTn}_1$: BC with a pair of hydrofoils (chord of 3.18 cm) positioned at height of $1/3 \times D$, swivel angle of $0^\circ$ and angle of attack of $10^\circ$.
- $\text{BCPTn}_2$: BC with a pair of hydrofoils (chord of 3.18 cm) positioned at height of $1/3 \times D$, swivel angle of $-20^\circ$ and angle of attack of $-10^\circ$.
- $\text{BCQ}_1$: BC with two pairs of hydrofoils—larger pair (chord of 3.18 cm) positioned at height of $1/6 \times D$, swivel angle of $0^\circ$ and angle of attack of $-10^\circ$ with a smaller pair (chord of 2.41 cm) at height of $1/3 \times D$, swivel angle of $60^\circ$ and angle of attack of $0^\circ$.

- $BCQ_2$: BC with two pairs of hydrofoils—larger pair (chord of 3.18 cm) positioned at height of $1/6 \times D$, swivel angle of $-20^\circ$ and angle of attack of $-10^\circ$ with a smaller pair (chord of 2.41 cm) at height of $5/12 \times D$, swivel angle of $70^\circ$ and angle of attack of $0^\circ$.

### 2.2. Tests in the towing tank

A series of free-vibration experiments were conducted (Farrell, 2007; Lee, 2007) in the MIT towing tank which has dimensions of 30 m × 2.4 m × 1.2 m. A carriage that can be driven along the length of the tank at a fixed speed by means of a servo motor is supported by both an overhead rail and a rail along the side of the tank. The carriage carries the testing equipment and provides an attachment point to which the test object may be mounted. The tests performed made use of a spring supported mounting system (Fig. 3) designed to provide free-response motion. An aluminum cylinder with a diameter of 7.6 cm and length of 200 cm was used. This cylinder had a wall thickness of 0.9 mm to help reduce the mass ratio of the system. It was mounted between two streamlined spars that pierce the surface of the water and hold the cylinder underwater. The system used linear roller bearings and linear motors to counter act any friction such as that due to any system misalignments. The motors were controlled using velocity feedback of the cylinder that was measured by a string velocity potentiometer. The spring system allows the transverse and inline directions to be tuned to two different natural frequencies (Dahl et al, 2006, 2007), however only motion in the transverse direction was allowed for this series of tests. The system incorporates a means of measuring forces and displacements. The displacements were measured using linear potentiometers attached to the main part of the carriage with the magnetic slider of the sensor attached to the freely moving rig. Voltages changes caused by the oscillating position of the slider were measured directly at 100 Hz by means of a data acquisition system. The forces were measured by Kistler three-axis piezoelectric force sensors located at the cylinder mounting points at the end of the spars.

Two different hydrofoil profiles were used in this set of tests. The first was a standard NACA63A010 section profile with an $a = 0.2$ camber line and will be referred to as the "flat hydrofoil". The second hydrofoil, referred to as the "curved hydrofoil", was designed with a camber line that follows the curvature of the cylinder. The maximum thickness of this foil was the same as that of the "flat hydrofoil". Aluminum molds of both hydrofoils with a span of 91.4 cm were manufactured. The hydrofoils were fabricated in these molds using a mixture of epoxy and milled fiberglass. Attachment rings with a thickness of 0.93 cm were attached to the cylinder at regular intervals. Streamlined aluminum extrusions were inserted between the hydrofoil and attachment rings to further offset the foils from the cylinder surface while reducing induced drag from the attachment screws.

Parameters of the foils that were varied include their orientation around the cylinder, their distance from the cylinder surface and whether the foils were staggered, single, or continuous. The orientation of the foil is defined by the angle ($\phi$) between the attachment screw and after centerline. The hydrofoils were tested at three angles: $90^\circ$, $75^\circ$ and $60^\circ$. Two distances ($d$) of the hydrofoil from the cylinder surface were tested: $0.33 \times R$ and $0.66 \times R$, where $R$ is the radius of the

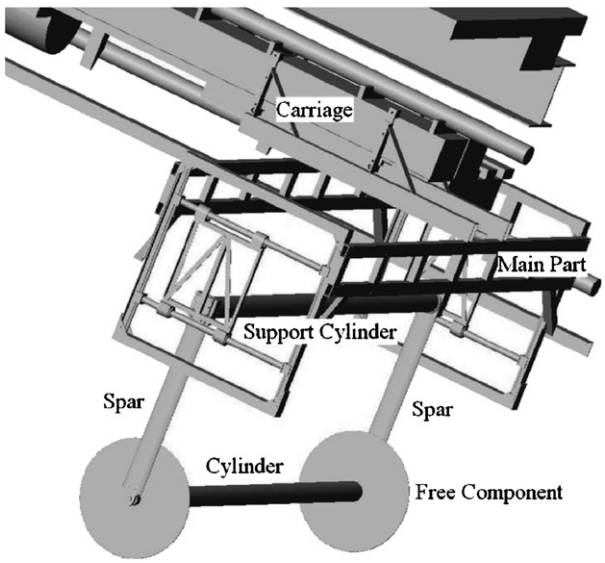


Fig. 3. Diagram of the free-response motion system used in towing tank tests.

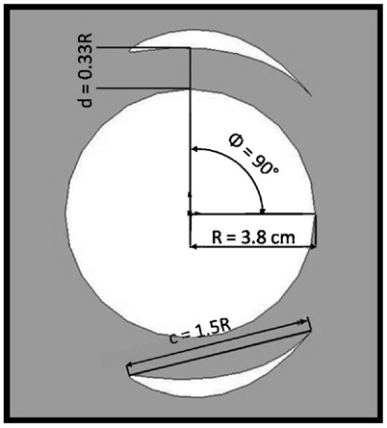


Fig. 4. Diagram of the C3 arrangement tested.

cylinder. The chord length ($c$) of the hydrofoils was equal to $1.5 \times R$. Each configuration was evaluated at eight different reduced velocities ranging from 4 to 14, thus, allowing for good resolution around the expected reduced velocities of vibration and a check on the higher reduced velocities for possible galloping response.

Tests in the towing tank were conducted at Reynolds number ranging from 20 000 to 80 000. The naming convention is such that the first letter refers to the type of hydrofoil being used with A representing the flat hydrofoils and C for the curved version. The number conveys the angle of attack, $\phi$, used. The angles 60°, 75° and 90° are denoted by the numbers 1, 2 and 3, respectively. The basic configurations tested are labeled as:

- A1: Flat hydrofoils with $d = 1/3 \times R$ and $\phi = 60°$.
- A2: Flat hydrofoils with $d = 1/3 \times R$ and $\phi = 75°$.
- C1: Curved hydrofoils with $d = 1/3 \times R$ and $\phi = 60°$.
- C2: Curved hydrofoils with $d = 1/3 \times R$ and $\phi = 75°$.
- C3: Curved hydrofoils with $d = 1/3 \times R$ and $\phi = 90°$ (see Fig. 4).

Further configurations were obtained through changes in the foil arrangements listed. A second letter of A at the end of the naming convention denotes a staggered configuration, i.e. foils were not continuous along the cylinder but consisted of a foil on one side of the cylinder followed by a similar foil on the opposite side, and so on. Hence, A1A, A2A, A3A, C3A, C1A, C2A refer to foil arrangement as in A1, A2, A3, C1, C2, C3, respectively, but in a staggered arrangement. Other configurations include:

- A3: Flat hydrofoils with $d = 1/3 \times R$ and $\phi = 90°$.
- A4: As in A1 but with a single foil extending the length of the cylinder on one side (asymmetric arrangement).
- A5: As in A2 but with a single foil extending the length of the cylinder on one side (asymmetric arrangement).
- C4: As in C1 but with a single foil extending the length of the cylinder on one side (asymmetric arrangement).
- C5: As in C2 but with a single foil extending the length of the cylinder on one side (asymmetric arrangement).
- C6: As in C3 but with a single foil extending the length of the cylinder on one side (asymmetric arrangement).
- D3: Curved hydrofoils with $D = 2/3 \times R$ and $\phi = 90°$.

## 3. Results and discussion

### 3.1. Vorticity and force analysis

The principal goal of using hydrofoils is to modify the flow about a cylinder so as to eliminate large-vortex formation, because it leads to unsteady forces on the body. Furthermore, a reduction in the drag force on the body was also sought. Forces in both the inline (drag) and transverse (lift) directions were recorded; these data were used in conjunction with PIV visualization to assess the success in modifying the flow.

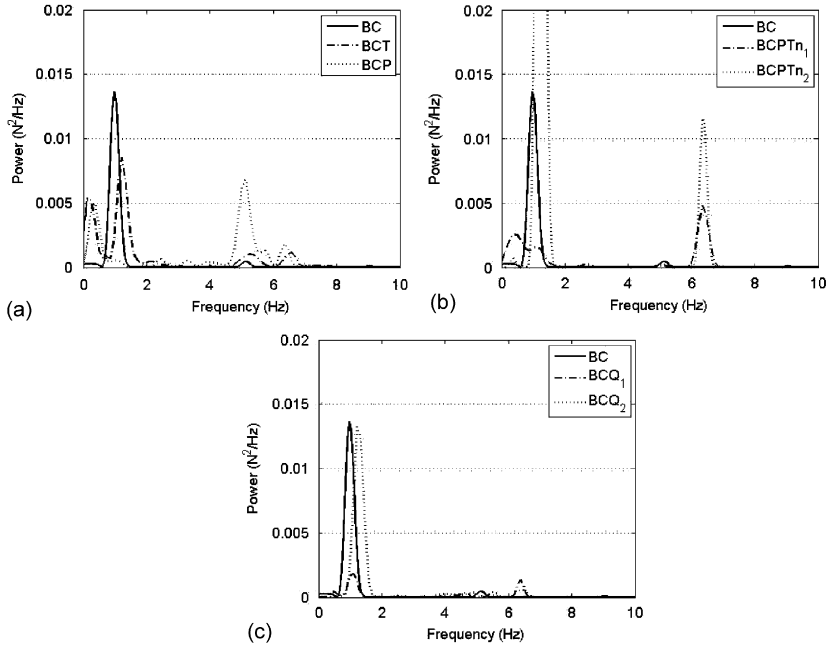


Fig. 5. Power spectra for various configurations showing both positive and negative changes in behavior.

First, a power spectral analysis on the lift force signal was performed to assess the intensity of the unsteady lift force; the minimization of the lift force fluctuations guided the selection of hydrofoil height, swivel angle and angle of attack. During the systematic variation of these three parameters, we found cases when the unsteady force was amplified considerably relative to the bare cylinder case, and others when the lift force was reduced; results for a few sample configurations are presented in Fig. 5. A predominant peak is often noted near the natural frequency of the unmodified system as denoted by the BC result. In some cases, this peak at the fundamental frequency is dramatically reduced. However, it is noted that a higher harmonic peak was often seen with the foil configurations.

The flow patterns behind a bare cylinder were used as the base case, against which comparisons were made. For this control case, typical alternating vortex shedding is seen with a corresponding peak in the PSD analysis at a Strouhal number of 0.2. A comparison of the vorticity field with the BCT configuration as depicted in Fig. 6 leads to the observation that constant streams of vorticity off of the structure occur without clear alternate shedding of vortices. However, the triangular fairing does not completely eliminate the unsteady lift force, as seen in Fig. 5. In fact, there is a dominant frequency lift component of comparable intensity to that measured for the bare cylinder. This can be explained by considering the mean behavior of the wake. In the first time capture, the wake bends downwards and then proceeds to straighten by the next time capture. Over the final two frames shown, the wake is seen to bend upwards. This cyclical flexing of the wake is seen throughout the remainder of the PIV images captured.

The PSD analysis of the lift signal for the $BCPTn_1$ configuration (Fig. 7) indicates minimal power at all frequencies. As with BCT, fairly consistent streams of vorticity of both rotational directions are seen to leave the structure. One apparent influence of the hydrofoils in this configuration is an infusion of leading-edge and trailing-edge vorticity, joining with the vortices being shed from the cylinder. This mingling of flow structures seems to cancel out patterned shedding and leads to a less coherent wake. Two factors appear to contribute to this interaction. First, the positive angle of attack acts to direct shedding from the hydrofoils into the immediate vicinity behind the cylinder. Secondly, the directing of vortices into this area is affected by the swivel angle of the foils. The trailing edges of the foils protrude to the back-end of the cylinder thus allowing for more direct influence in the near-wake region. The overall behavior of the wake remains fairly constricted and does not exhibit the flexing behavior as mentioned for the triangular fairing case.

In the $BCPTn_2$ case alternating vortex shedding is seen, similar to that for the bare cylinder, but to a far lesser extent. A notable difference is that the vortices wrap around the back-end of the cylinder and remain closer to its surface. This is coupled with a higher power spike in the PSD; hence, pushing the hydrofoils forward and orienting them with a negative angle of attack reduces their influence on the wake. Furthermore, a negative angle of attack has two results; the vorticity being shed off of the foils is weaker and not directed into the wake region directly behind the cylinder.

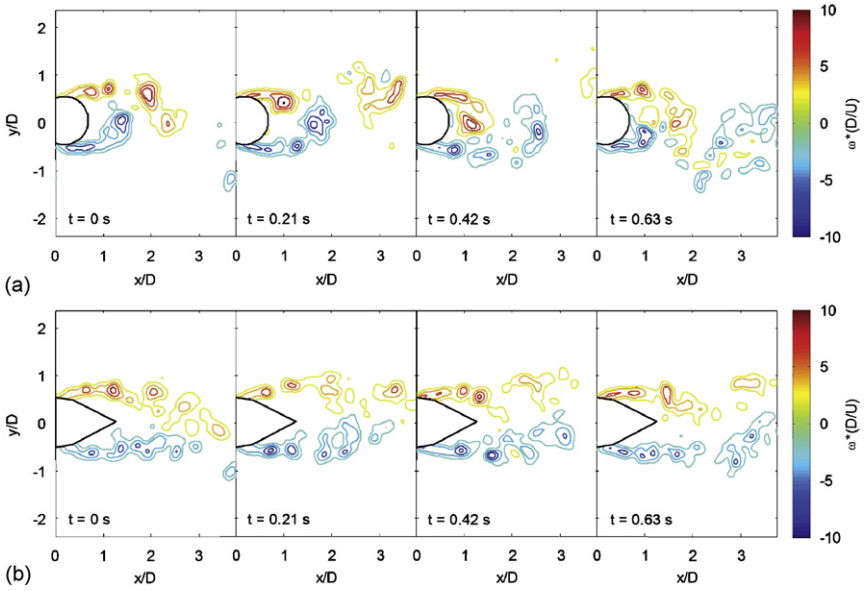


Fig. 6. Time separated vorticity fields for the (a) BC and (b) BCT configurations.

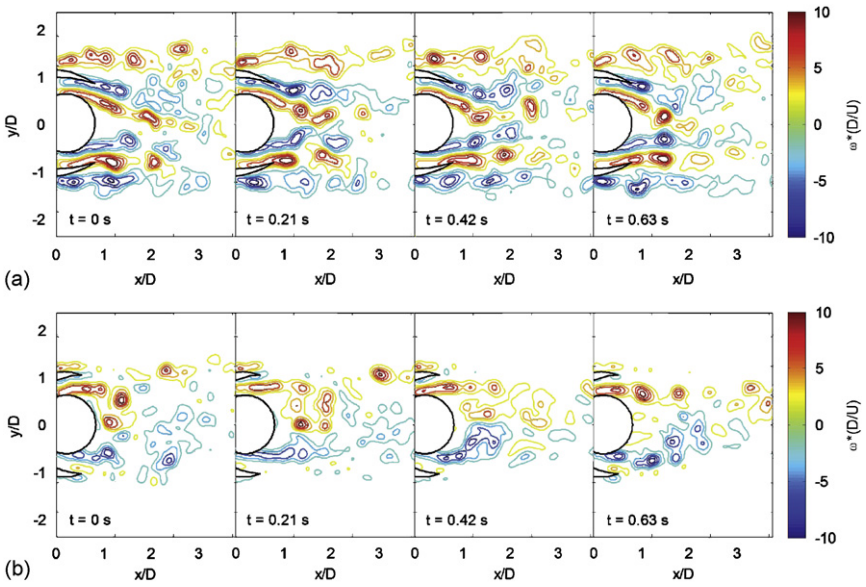


Fig. 7. Time separated vorticity fields for the (a) $BCPTn_1$ and (b) $BCPTn_2$ configurations.

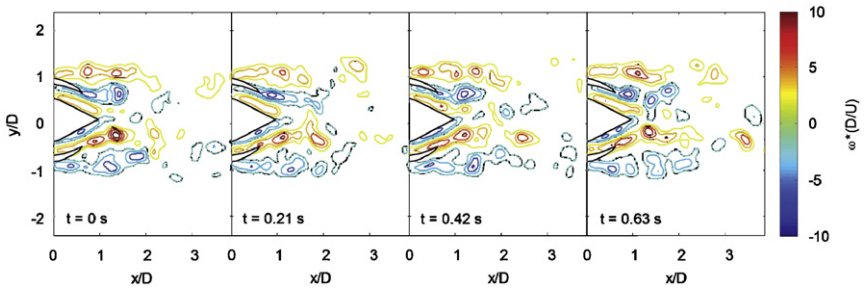


Fig. 8. Time separated vorticity fields for the BCP configuration.

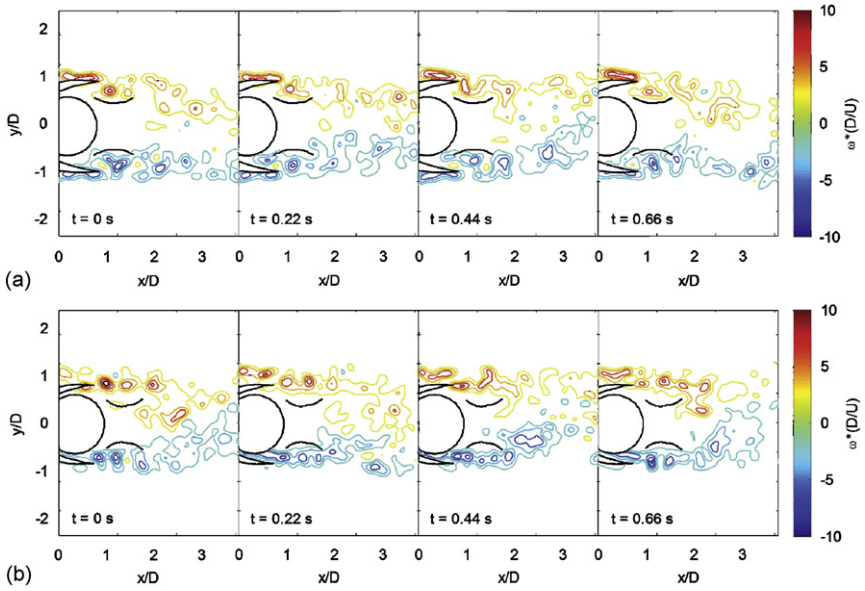


Fig. 9. Time separated vorticity fields for the (a) $BCQ_1$ and (b) $BCQ_2$ configurations.

This configuration does not interfere with vortex shedding from the cylinder, but instead seems to amplify its effects on the oscillations of the lift force experienced by the structure.

A change in flow behavior is recognized in the case where the triangular fairing is combined with the hydrofoils (BCP). The case shown in Fig. 8 is typical of this configuration. Generally, vorticity was seen to shed in streaks. Analysis of the PSD does not show a strong fundamental frequency of oscillation in the force signal, although a peak at a higher frequency is noted.

Two sets of PIV images from quad-foil configurations are shown in Fig. 9 to demonstrate the effect of parameter adjustment on this configuration. The $BCQ_1$ configuration, for which the larger foils are located further back, with a swivel angle of zero degrees, shows a reduction in the intensity of lift signal fluctuations. Again, having the foils positioned further back allows for the flow structures from the foil tips to best interact with the cylinder wake. Furthermore, with the additional foils of smaller chord length now present, vorticity is shed from the set of larger foils and remains separated from the region located directly behind the cylinder. This leads to less significant influencing of the cylinder itself from these flow structures. It is noted again that the wake pattern fluctuates upwards and downwards as described for the BCT configuration. Nevertheless, this occurs at a fairly minimal level and leads to little power content in the PSD of the lift signal.

The $BCQ_2$ foil configuration for which the large foils have been moved forward to a swivel angle of 20° exhibits different results. The smaller chord hydrofoils have also been moved slightly closer to one another with the adjustment of the swivel angle to 70°. For this case, the vortices that shed off the larger foils again are guided by the smaller foils but wrap around to enter the relatively stagnant region between the two smaller hydrofoils aft of the cylinder. This wrap around occurs in a periodic fashion which leads to a fluctuating lift signal suggesting forcing of the cylinder that could lead to VIV behavior.

Drag reduction was also investigated for the foil modified cylinders. The mean drag coefficient ratios between the modified configurations and the bare cylinder are shown in Fig. 10. The drag coefficient for the control case, BC, is labeled as $C_{Do}$ and has a value of 1.33. A reduction of approximately 15% was seen for the BCT modification. Reductions in drag differed for each type of cylinder modification with variations depending on the chosen parameters of foil height, swivel and angle of attack. Some cases led to an increase, but most resulted in drag reduction. Overall, the greatest benefits were seen for the BCP configurations with a maximum reduction of 48%.

### 3.2. Higher Reynolds number testing with free-vibration apparatus

The cross-flow motion results presented in Fig. 11 show that properly designed hydrofoils lead to a reduction in VIV and can even eliminate the phenomenon altogether. The configuration labeled C3 is shown to perform poorly, but the

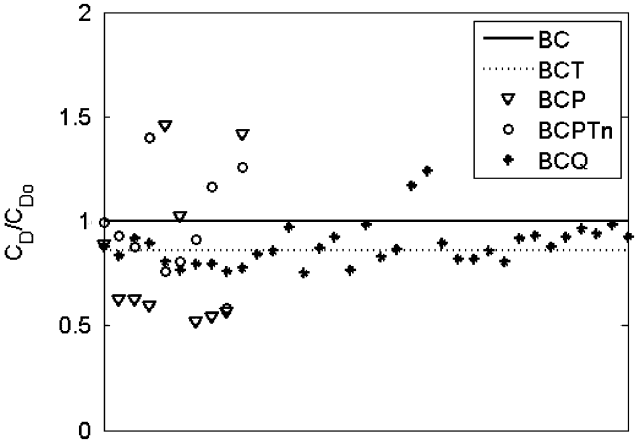


Fig. 10. Drag ratios relative to BC results for the configurations tested.

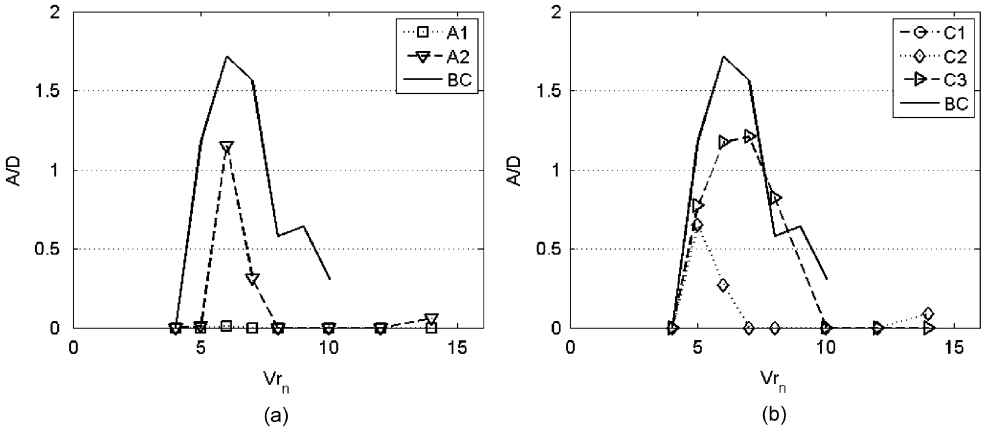


Fig. 11. Results of tests performed in the towing tank with a pair of continuous foils mounted on a rigid cylinder.

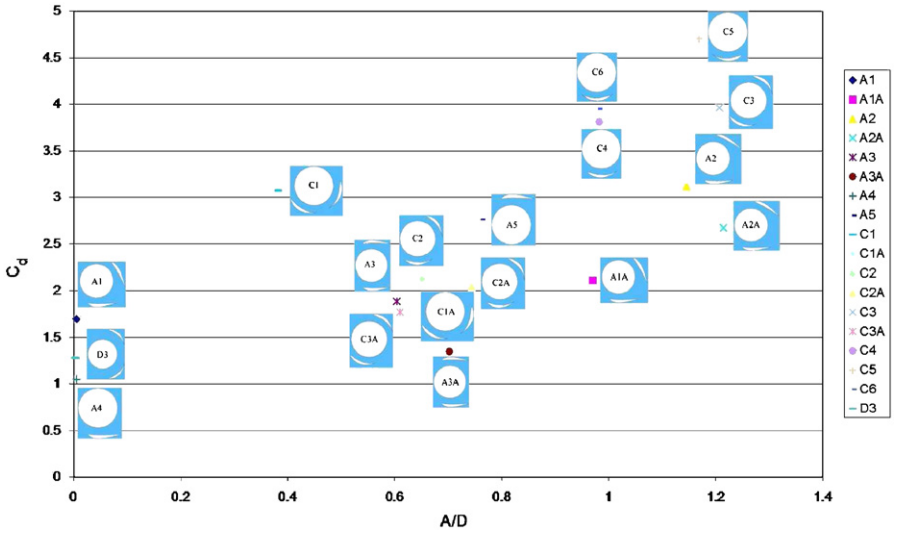


Fig. 12. Drag coefficient determined from forces on structure when at its maximum oscillation amplitude.

noteworthy observation is that all other configurations show marked improvement, leading to significant reduction in amplitude of response. Significant reductions in the amplitude oscillation are noted for the A1 and C1 configurations with modest reductions seen for A2 and C2. Furthermore, the region of sustained oscillatory behavior of the cylinder is confined to a more narrow band of reduced velocities. These results provide confirmation that properly positioned foils can lead to minimal vibrations as suggested by reductions in lift force oscillations in the small towing tank tests.

A reduction in the drag coefficient as a result of the attachment of foils to the cylinder is seen in the large towing tank tests. The time-averaged drag coefficient results versus the maximum amplitude of vibration recorded for all reduced velocities are shown in Fig. 12. The depictions in the figure illustrate the positions of the hydrofoils for the respective data point. The value of the drag coefficient for the bare cylinder tested in the free-vibration apparatus at a reduced velocity leading to maximum oscillation was measured to be 3.7. The extent of drag reduction from hydrofoil modification covers a wide range, but most configurations are shown to have led to reductions. Significant improvements are seen for many cases including configuration A1 which was previously noted to exhibit almost no VIV response. Configuration A4 which consisted of a single foil in an asymmetric arrangement also exhibited no VIV and the lowest maximum drag coefficient with a value below 0.70.

## 4. Conclusion

It is shown that properly positioned foils can significantly alter the flow around a circular cylinder to eliminate VIV and reduce drag. Although the resulting flow patterns exhibit reduction in unsteadiness and overall wake width, complex patterns persist as foil-induced vorticity mixes in with the cylinder-shed shear layers. Still, we can claim that the goal to make flow behavior closer to potential-flow patterns is a good guiding principle to eliminate VIV while also reducing drag. The first use of a smaller tank to test the effect of the foils by measuring forces and obtaining whole-field flow visualization through PIV, allowed a fast parametric search and was crucial in identifying optimal solutions. The final testing of the cylinder with attached foils in free vibrations performed in the towing tank confirmed the predictions. Under optimal conditions VIV is eliminated for all reduced velocities while a drag coefficient in the range between 0.50 and 0.70 is feasible under sub-critical conditions.

## Acknowledgment

The authors acknowledge with gratitude financial support by BP.

## References

Bearman, P.W., 1984. Vortex shedding from oscillating bluff bodies. Annual Review of Fluid Mechanics 16, 195–222.

Dahl, J.M., Hover, F.S., Triantafyllou, M.S., 2006. Two-degree-of-freedom vortex-induced vibrations using a force assisted apparatus. Journal of Fluids and Structures 22, 807–818.

Dahl, J.M., Hover, F.S., Triantafyllou, M.S., 2007. Resonant vibrations of bluff bodies cause multi-vortex shedding. Physical Review Letters 99, 144503.

Every, M.J., King, R., Weaver, D.S., 1982. Vortex-excited vibrations of cylinders and cables and their suppression. Ocean Engineering 9, 135–157.

Farrell, D.E., 2007. Vortex induced vibrations of a cylinder: experiments in reducing drag. SM Thesis, Mechanical Engineering Department, Massachusetts Institute of Technology, Cambridge, MA, USA.

Grimminger, G., 1945. The effect of rigid guide vanes on the vibration and drag of a towed circular cylinder. David Taylor Model Basin, USA.

Hoerner, X., Sighard, F., 1992. Fluid Dynamic Drag. Hoerner Fluid Dynamics, CA, USA.

Jacobsen, V., 1996. Vibration suppression devices for long, slender tubulars. In: Offshore Technology Conference, Paper 8156, Houston, TX, USA.

Lee, E.J., 2007. Airfoil vortex induced vibration suppression devices. SM Thesis, Mechanical Engineering Department, Massachusetts Institute of Technology, Cambridge, MA, USA.

Sarpkaya, T., 1979. Vortex-induced oscillations. Journal of Applied Mechanics 46, 241–257.

Sarpkaya, T., 2004. A critical review of the intrinsic nature of vortex-induced vibrations. Journal of Fluids and Structures 19, 389–447.

Strykowski, P.J., Sreenivasan, K.R., 1990. On the formation and suppression of vortex shedding at low Reynolds numbers. Journal of Fluid Mechanics 218, 71–107.

Triantafyllou, M.S., Hover, F.S., Yue, D.K.P., 2003. Vortex-induced vibrations of slender structures in shear flow. In: Benaroya, H., Wei, T. (Eds.), Proceedings of the IUTAM Symposium on Coupled Fluid-Structure Interaction Using Analysis, Computations and Experiments, Rutgers, NJ, USA, Paper 1–6.

Willert, C.E., Gharib, M., 1991. Digital particle image velocimetry. Experiments in Fluids 10, 181–193.
Williamson, C.H.K., Govardhan, R., 2004. Vortex-induced vibrations. Annual Review of Fluid Mechanics 36, 413–455.
Zdravkovich, M.M., 1980. Review and classification of various aerodynamic and hydrodynamic means of suppressing vortex shedding. Journal of Wind Engineering and Industrial Aerodynamics 7, 145–189.
Zdravkovich, M.M., 1997. Flow Around Circular Cylinders, vols. 1 and 2. Oxford University Press, Oxford, UK.